THE INFLUENCE OF SLOPE ROUGHNESS ON LATERAL DISPERSION OF ROCKFALL

Gaoyuan LYU [1] and Kiyonobu KASAMA [2]

[1] Faculty of Engineering, Kyushu University (Nishiku Motooka 744, Fukuoka 819-0395, Japan)
E-mail: lyu.gaoyuan.740@s.kyushu-u.ac.jp
[2] Faculty of Engineering, Kyushu University (Nishiku Motooka 744, Fukuoka 819-0395, Japan)
E-mail: kasama@civil.kyushu-u.ac.jp

Key Words: *rockfall, slope roughness, lateral dispersion, Monte Carlo Simulation*

1. INTRODUCTION

Rockfall movement is uncontrollable and has a significant impact on transportation infrastructure such as highways and railways, as well as private houses. Reports indicate that more than 200 out injuries caused by rockfall and slope failures in 2016 Kumamoto Earthquake, causing severe economic losses and loss of life and safety [1]. The lateral dispersion of rockfall trajectories is a crucial indicator for disaster preparedness and prevention. It is influenced by numerous complex factors, which can be grouped into four categories: the source of the rockfall (e.g., location information), the characteristics of the rockfall (e.g., material properties, shape), the initial conditions (e.g., direction), and the characteristics of the slope (e.g., material properties, topography, roughness) [2]. Previous studies have concluded that slope roughness significantly affects the randomness of rockfall trajectories, as each collision between the rockfall and the slope is a randomized process. Researchers such as Crosta et al.[3] and Nishimura et al.[4], by introducing a normal distribution to represent roughness and considering factors such as the average slope angle and rock shape, found that roughness increases the lateral dispersion of rockfalls. However, the spatial correlation of slope roughness has been rarely considered in past studies. For instance, slope roughness varies spatially, being lower in some areas and higher in others, which becomes a causal factor in the random variation of rockfall trajectories.

To reasonably account for slope roughness, a probabilistic analysis is conducted to investigate the influence of roughness on the lateral dispersion of rockfall trajectory along the slope.

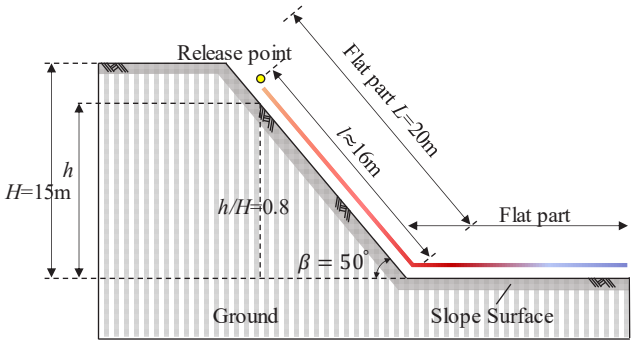

Fig. 1 Typical slope model in this study.

2. ROCKFALL MODELLING

A rockfall numerical model used in this study is depicted in Fig. 1. In this model, a slope angle of 50° and a length of 20 m is assumed reflecting typical rockfall hazard scenarios in mountainous countries such as Japan[5]. The rockfall simulation involves a free-falling phase at a height of 2 m from the slope surface. The length from the initial contact location to the slope toe is 16 m. According to the past database[6], the size of rock varies from cmmeters to meters while size with the high frequency is in a range of 0.4 ~ 0.6 m. In this study, the rockfall is modeled as a sphere with a diameter of 0.5 m.

3. DISCRETE ELEMENT METHOD

(1) A summary of DCDEM

The simulation tool in this study is selected as the Distributed Contact Discrete Element Method (DCDEM) because of its effectiveness in collision

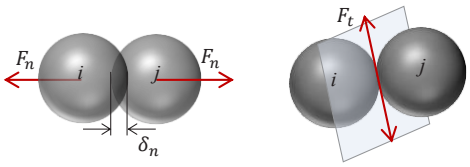

Fig. 2 Contact model in DCDEM.

simulations for solid contact, which has been validated in numerous studies[7]. In DCDEM, particle distance is uniform to improve computational efficiency[8)9)]. The slope and the rockfall are constructed by assembling a group of particles of uniform radius, and the relative displacement is ensured unchanged to represent a solid. The contacts in slope-rock are governed by Newton's second law, which combines the forces of each particle in the rock or slope to determine the resultant force acting on the corresponding object.

$$M_I \frac{d\boldsymbol{V}_I}{dt} = \sum_{k\in I} m_k \frac{d\boldsymbol{v}_k}{dt} \quad (1)$$

$$\boldsymbol{I}_I \frac{d\boldsymbol{\Omega}_I}{dt} = \sum_{k\in I} m_k(\boldsymbol{r}_k - \boldsymbol{R}_I) \times \frac{d\boldsymbol{v}_k}{dt} \quad (2)$$

where object I possess a mass M_I, velocity $\boldsymbol{V}_I$, inertial tensor $\boldsymbol{I}_I$, angular velocity $\boldsymbol{\Omega}_I$ and center of gravity $\boldsymbol{R}_I$. The vectorial quantities are computed at every time step dt.

The concept of the contact model for rock particles and slope particles is illustrated in Fig. 2. The $\boldsymbol{F}_{n,ij}$ is the normal force and $\boldsymbol{F}_{t,ij}$ is the tangential force between two particles from the rockfall and the slope, respectively. Each direction is controlled by a spring and a damper. In each direction, the force is linearly related to the deformation and the damper acts as a penalty term to control the energy dissipation caused by deformation as follows:

$$\boldsymbol{F}_{n,ij} = k_{n.ij} \cdot \delta_{ij}^{n\frac{3}{2}} \cdot \boldsymbol{e}_{ij}^{n} - \gamma_{n.ij} \cdot \delta_{ij}^{n\frac{1}{4}} \cdot v_{n,ij} \cdot \boldsymbol{e}_{ij}^{n} \quad (3)$$

$$\boldsymbol{F}_{t,ij} = \frac{2}{7} k_{n,ij} \cdot \delta_{ij}^{t} \cdot \boldsymbol{e}_{ij}^{t} \cdot v_{t,ij} - \frac{2}{7} \gamma_{n,ij} \cdot \delta_{ij}^{t} \cdot \boldsymbol{e}_{ij}^{t} \cdot v_{t,ij} \quad (4a)$$

where $k_{n.ij}$ is the contact stiffness, $\gamma_{n.ij}$ is the damping coefficient, δ_{ij} is the overlap, $v_{n,ij}$ is the normal velocity, and $\boldsymbol{e}_{ij}^{n}$ is the normal vector between the two interacting particles i and j from the rock and the slope, respectively. A Coulomb-like slip model is applied to impose a limit on the magnitude of the tangential force, $\boldsymbol{F}_{t,ij}$ and calculated as follows:

$$\left|\boldsymbol{F}_{t,ij}\right| \le \mu_{f,ij} \left|F_{n,ij}\right| \tan\varphi \quad (4b)$$

where φ corresponds to the normal velocity and $\mu_{f,ij}$ is the kinetic friction coefficient between rockfall and slope.

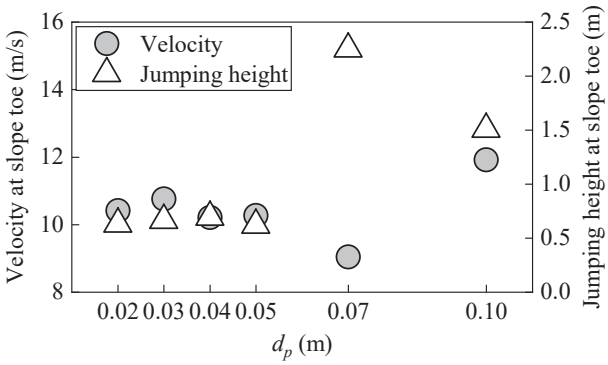

Fig. 3 Calculation accuracy due to particle distances d_p.

(2) Accuracy of particle distance

Particle distance (d_p) and overlap ratio (OR) are two parameters affecting shape representation in DCDEM. Smaller d_p and larger OR leads to more accurate calculation results, however, the number of particles will be increased greatly with lower computational efficiency. In this study, the OR is fixed at 1 based on the previous literature[10], meaning no initial overlap between initial particles. As shown in Fig. 3, d_p is adjusted from 0.02 m to 0.10 m to check the variation of calculation results. A comparison of the velocity and jump height at the slope toe reveals that calculation results are stable until $d_p \le 0.05$ m, while results fluctuate considerably when $d_p > 0.05$ m. Referred to this, this study sets the particle distance d_p to 0.05 m.

4. REPRESENTATION OF ROUGHNESS

The random field theory is used to represent the spatial variability[11] for a surface roughness $\boldsymbol{r}(x, y, z = 0)$ which is represented as the sum of the trend component (mean) and the random component (deviation from the mean):

$$\boldsymbol{r}(x,y) = \boldsymbol{t}(x,y) + \boldsymbol{\epsilon}(x,y) \quad (5)$$

where $\boldsymbol{r}(x,y)$ is the value at coordinate (x,y), $\boldsymbol{t}(x,y)$ is the value of the trend component at (x,y), which is a deterministic value, and $\boldsymbol{\epsilon}(x,y)$ is the random component at (x,y) which is the static random field vector. In order to consider the correlation spatially, an exponential autocorrelation function is used:

$$\rho_{(ij)} = exp\left(-\frac{2|\Delta i|}{\theta_i} - \frac{2|\Delta j|}{\theta_j}\right) \quad (6)$$

where Δi and Δj refer to the lag distance in row and column in a matrix, respectively, with their corresponding autocorrelation length θ_i and θ_j. Larger autocorrelation lengths signify correlations

over extended lengths. Ω consists of a matrix of autocorrelation coefficients ρ at different locations

$$\Omega = \begin{bmatrix} 1 & \rho_{12} & \cdots & \rho_{1n} \\ \rho_{12} & 1 & \cdots & \rho_{2n} \\ \vdots & \vdots & \ddots & \vdots \\ \rho_{1n} & \rho_{2n} & \cdots & 1 \end{bmatrix} \quad (7)$$

where n is the number of the random numbers. Then, Cholesky decomposition for Ω is conducted to obtain the transpose matrix S^T with its own matrix S.

$$\Omega = S^T S \quad (8)$$

To write the correlation matrix into a random field, multiply by a distribution such as normal distribution.

$$\boldsymbol{\epsilon} = S^T R \quad (9)$$

where R is the random number from the prescribed distribution. Finally, the creation of a random field $\boldsymbol{\epsilon}$ considering spatial correlation length is completed.

(1) Intensity

In this study, a location is investigated to provide the reference of parameter design for slope roughness. The investigated location is shown in Fig. 4. The result shows that a normal distribution is well fitted

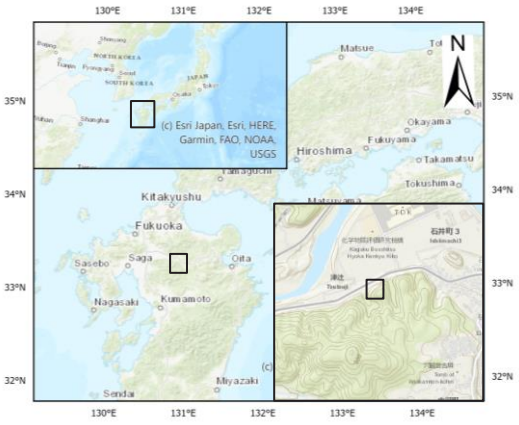

Fig. 4 Investigated location for slope roughness.

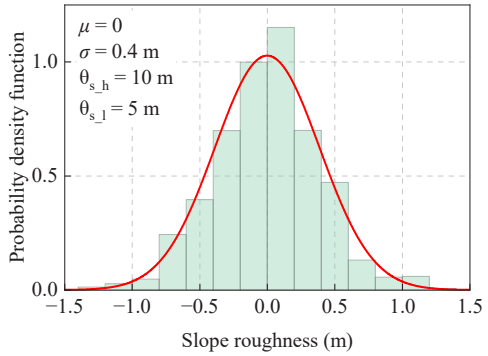

Fig. 5 Statistic results from the investigated location.

and that standard deviation σ is 0.4 m, θ_{s_h} is around 10 m and θ_{s_l} is around 5 m as shown in Fig. 5. This study explores the effects of parameter variations based on this results. Fig. 5 illustrates the roughness distribution with a standard deviation σ of 0.4 m on a surface measuring 60 m horizontally and 20 m longitudinally. Red regions represent bumps and blue regions represent depressions, with a grid resolution of 1 m.

(2) Spatial correlation

The distribution of roughness in Fig. 6 is random without consideration of spatial correlation. By assuming an autocorrelation length in the horizontal direction $\theta_{s\_h} = 10$ m and in the longitudinal direction $\theta_{s\_l} = 5$ m with a standard deviation σ of 0.4 m, the roughness generation with the consideration of spatial correlation is achieved as shown in Fig. 7.

It is worth noting that the random field (Fig.8 (a)) is discrete with 1-m resolution, and a continuous surface (Fig. 8 (b)) is transformed using spline algorithm[10] fitted to the discrete random field, which is then rotated by 50° to match the slope surface in the rockfall numerical modeling as shown in Fig. 8 (c). Fig. 8 (d) is the slope numerical modeling with roughness and is subsequently imported into DualSPHysics software for DCDEM calculation with its corresponding visualization as shown in Fig. 8 (e).

In this study, standard deviation σ is varied in a range of 0 m ~ 1.0 m, autocorrelation length in the horizontal direction θ_{s_h} of 5 m ~ 15 m and autocorrelation length in the longitudinal direction θ_{s_l} of 2 m ~ 8 m. For each parameter, 100 slopes are

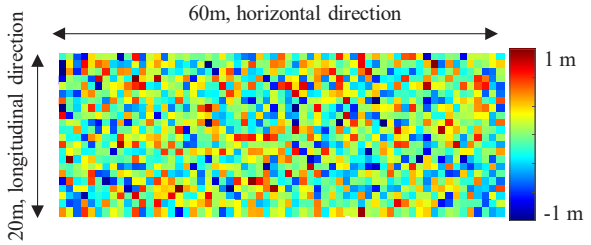

Fig. 6 A random field with $\sigma = 0.4$ m while without θ_{s_l} and θ_{s_h}.

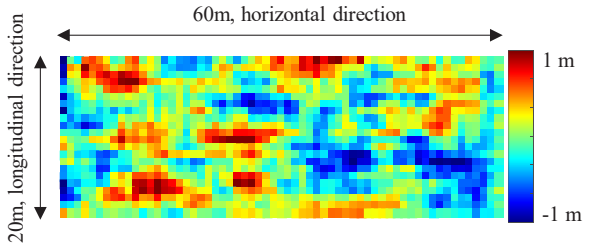

Fig. 7 A random field with $\sigma = 0.4$ m while $\theta_{s\_l} = 5$ m and $\theta_{s\_h} = 10$ m.

Table 1 Input parameters for slope roughness.

Parameter	Value	Number of MCS
σ (m)	0 ~ 1.0 m	100
θ_{s_l} (m)	2 ~ 8 m	
θ_{s_h} (m)	5 ~ 15 m	

σ: standard deviation for slope roughness;
θ_{s_l}: longitudinal autocorrelation length for slope roughness;
θ_{s_h}: horizontal autocorrelation length for slope roughness;

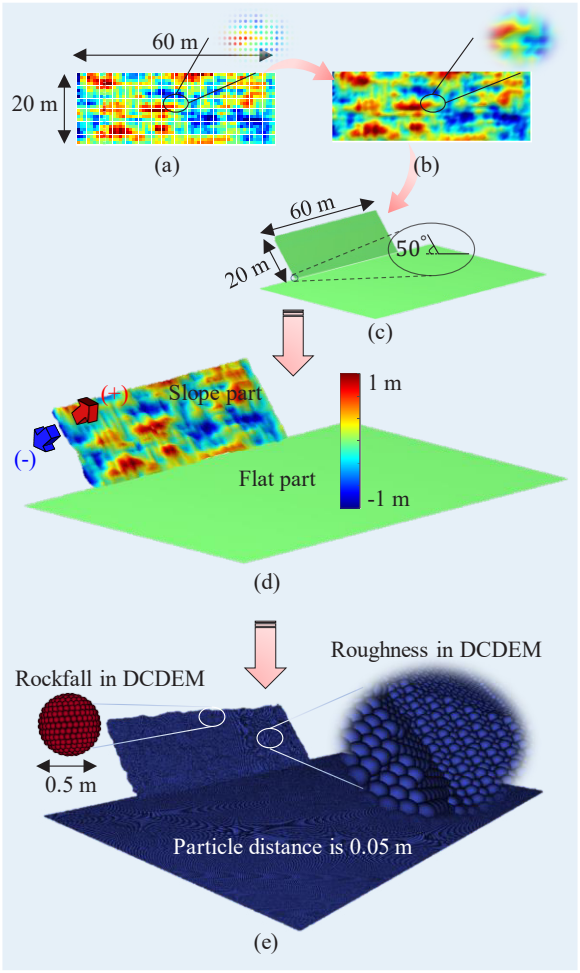

Fig. 8 Sketch of roughness generation for slope numerical modeling.

generated based on the Monte Carlo Simulation (MCS). All input parameters are listed in Table 1.

5.PROBABILISTIC EVAUATION

In order to evaluate rockfall trajectory probabilistically, a reach probability map of rockfall is calculated. The space is divided into a 1-m grid and count the number of passing rockfalls for each grid. The reach reach probability for each grid is as follows:

$$P_{ij} = \frac{N_{ij}}{n} \tag{10}$$

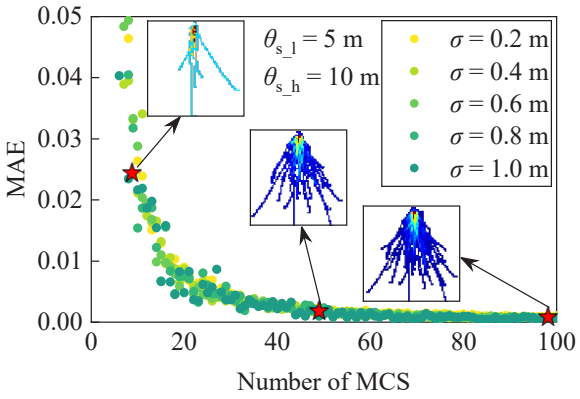

Fig. 9 The relationship between MAE and the of number of MCS with σ = 0.2 ~1.0 m at fixing θ_{s_l} = 5 m and θ_{s_h} = 10 m.

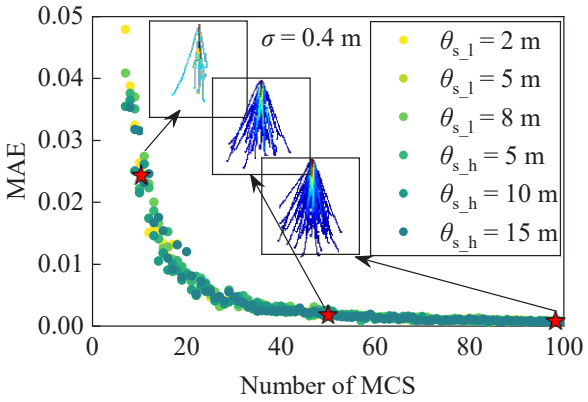

Fig. 10 The relationship between MAE and the of number of MCS with θ_{s_l} = 2 ~ 8 m and θ_{s_h} = 5 ~ 15 m at fixing σ = 0.4 m.

where P_{ij} is the reach reach probability for grid ij with n MCS, i is the row number, j is the column number, and N_i is the counted rock number in grid ij with n MCS. Fig. 9 is given as an example. It is worth noting that the colormap range has been adjusted to 0 ~ 0.3 for clear viewing, with red color representing high reach probability and blue color representing low reach probability.

(1) Number of simulations

In order to explore the changes in the reach reach probability with MCS, the mean absolute error, MAE[12], is calculated as:

$$\mathrm{MAE} = \frac{\sum_i \sum_j |P_{ij,n} - P_{ij,n-1}|}{m} \tag{11}$$

where $P_{ij,n}$ is the reach reach probability in grid ij with n MCS, $P_{ij,n-1}$ is the reach reach probability in grid ij with n-1 MCS, and m is the total number of grids of reached rockfall, which reflects the affected area by rockfall. The relationship between MAE and the number of MCS for a given σ is illustrated in Fig. 9. It is observed that when the number of

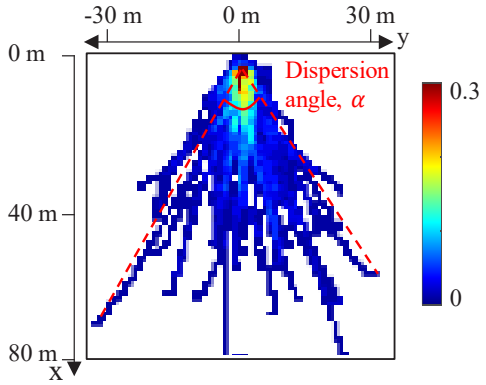

Fig. 11 Reach reach probability under the slope roughness with $\sigma = 0.4$ m, $\theta_{s\_l} = 5$ m and $\theta_{s\_h} = 10$ m.

simulations reaches 100, MAE all approaches 0.001 MAE, indicating the reach probability map obtained through 100 simulations is probabilistically reliable within the 0.001 MAE. Similar numerical findings can be observed in Fig. 10 for autocorrelation length variations. Therefore, 100 simulations can ensure the stability of the reach probability map within 0.001 MAE considering the slope roughness.

(2) Dispersion angle

As shown in Fig. 11, the initial release location of the rockfall ($x = 3$ m, $y = 0$ m), along with the two farthest locations it reaches laterally (along the y-axis), form the dispersion angle, denoted by α, which is used as an index to represent the lateral dispersion for rockfall movement. Fig 12 shows changes in α under intensity variation of σ, while Fig. 13 and Fig. 14 show changes under α in the variation of horizontal autocorrelation length θ_{s_h} and longitudinal autocorrelation length θ_{s_l}.

In Fig. 12, when σ is 0, representing the slope without any roughness, there is no dispersion angle. With increasing the σ, the roughness promotes the lateral dispersion of the rockfall trajectory. When σ is 0.2 m, the α is 48°. The α increases to 52° at σ = 0.4 m. Beyond this, the α fluctuates between 64° and 79° with increasing σ from 0.6 m to 1.0 m. It is indicated that the σ is positively correlated with the α and there is a maximum α around 75°.

In Fig. 13, with increasing the θ_{s_h}, α shows an decreasing trend. When θ_{s_h} = 5 m, α is 59°; when θ_{s_h} = 10 m, α is 52°; when θ_{s_h} = 10 m, α is 45°.

In Fig. 14, with increasing the θ_{s_l}, α shows an decreasing trend. When θ_{s_l} = 2 m, α is 65°; when θ_{s_l} = 10 m, α is 52°; when θ_{s_l} = 10 m, α is 51°.

Fig. 15 shows the all result of the dispersion angle under parameter variation for slope roughness. The variation of σ shows a significant influence on the dispersion angle than other two parameters θ_{s_h} and θ_{s_l} because the dispersion angle ranges in the

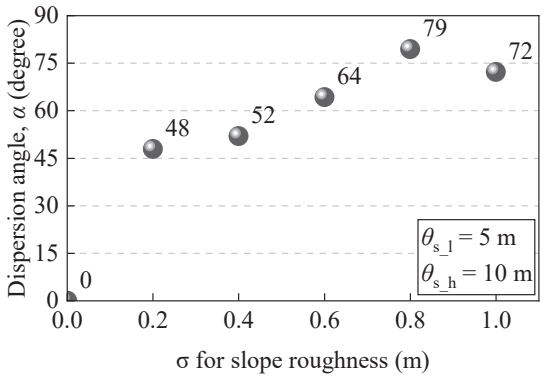

Fig. 12 Dispersion angle α with $\sigma = 0 \sim 1.0$ m while fixing $\theta_{s\_l} = 5$ m and $\theta_{s\_h} = 10$ m.

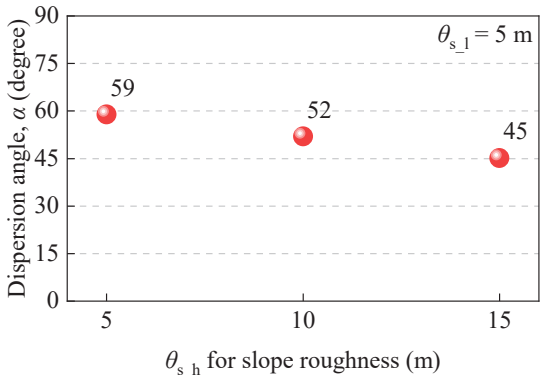

Fig. 13 Dispersion angle α with $\theta_{s\_l} = 2 \sim 8$ m while fixing $\theta_{s\_h} = 10$ m and $\sigma = 0.4$ m.

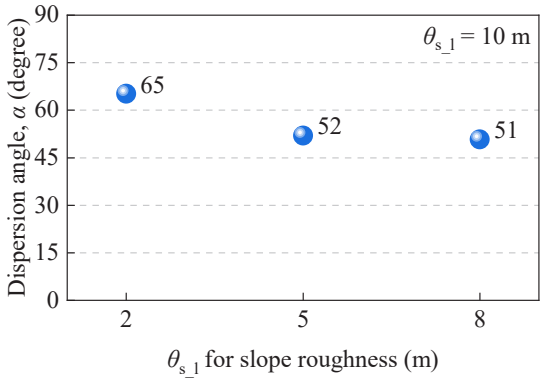

Fig. 14 Dispersion angle α with $\theta_{s\_h} = 5 \sim 15$ m while fixing $\theta_{s\_l} = 5$ m and $\sigma = 0.4$ m.

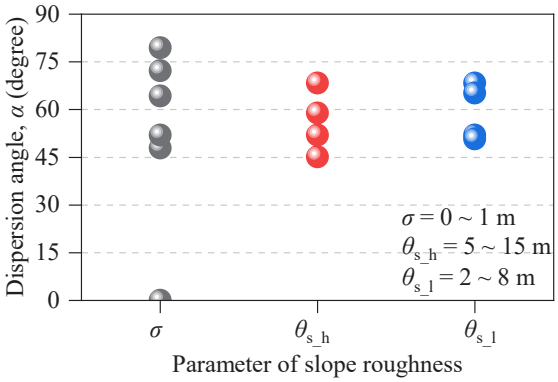

Fig. 15 Results of dispersion angle α with $\sigma = 0 \sim 1\,m$, $\theta_{s\_h} = 5 \sim 15$ m and $\theta_{s\_l} = 2 \sim 8$ m.

largest variation of 0 ~ 79° while in the variation of 45 ~ 70° under variation of θ_{s_h} and θ_{s_l}.

6. CONCLUSIONS

The slope roughness is represented using the random field theory, controlled by 3 parameters for intensity and spatial correlation: standard deviation σ for intensity, longitudinal autocorrelation length of θ_{s_l} and horizontal autocorrelation length θ_{s_h} for spatial correlation. With the help of the numerical tool of the Distributed Contact Discrete Element Method (DCDEM), the reach probability map of the rockfall trajectory is calculated and the dispersion angle is statistic . The main findings are as follows:

(1) Considering the trajectory variation due to slope roughness, 100 simulation can obtain a reach probability within 0.001 of MAE.
(2) The intensity of slope roughness σ promotes the lateral dispersion of rockfall trajectory. The dispersion angle is varied from 0° to 79° with σ increasing from 0 m to 1.0 m.
(3) As increasing of θ_{s_l} from 2 ~ 8 m and and θ_{s_h} from 5 ~ 15 m, the dispersion angle varies from 45° ~ 70°.
(4) Compraed to θ_{s_l} and θ_{s_h}, σ has more significant influence on the dispersion angle than spatial correlation.
(5) When σ exceeds the 0.4 m, dispersion angle shows a stable trend around 75°.

Except slope roughness, the effect of the rock shape on the trajectory variation is also significant. In this study, the rock is simulated as a sphere to eliminate the rock shape effect with its initial angle. In the subsequent study, the rock shape effect with its initial angle will be considered.

REFERENCES

1) Ministry of Land, Infrastructure, Transport and Tourism.
2) Li, L., Lan, H.: Probabilistic modeling of rockfall trajectories: a review. Bull. Eng. *Geol. Environ*. Vol. 74, 1163–1176, 2015.
3) Lu Z., Zhiyuan Z., Qi W., Kaihui R., Yihan W., Wei W. and Hong Z.: A Stochastic Rockfall Model Related to Random Ground Roughness Based on Three-Dimensional Discontinuous Deformation Analysis, Frontiers in Earth Science, Vol. 9, 2021.
4) Tsuyoshi N., Tsuyoshi F. and Hideo K.: Numerical simulation of effects of slope micro-topography on rockfall trajectories, *Journal of the Society of Materials Science*, Vol. 59, No. 3, pp. 199-204, 2010.
5) Nakatani H., Takiguchi S. and Kanazawa A.: Reality of cliff failure disaster, *TECHNICAL NOTE of National Institute for Land and Infrastructure Management*, No. 1122, 2020.
6) Japan-Road-Association, *Maruzen Publisher*, Tokyo, 2017.
7) see https://dual.sphysics.org/.
8) Ricardo, B. C., Alejandro, J.C. C., Jose, M. D., Rui, M.L.F. and Moncho, G.: SPH–DCDEM model for arbitrary geometries in free surface solid–fluid flows, *Computer Physics Communications*, Vol. 202, pp. 131-140, 2016.
9) Klaus Thoeni, Anna Giacomini, Cédric Lambert, Scott W. Sloan, John P. Carter, A 3D discrete element modelling approach for rockfall analysis with drapery systems, *International Journal of Rock Mechanics and Mining Sciences*, Vol. 68, pp. 107-119, 2014.
10) Ikkoh T., Shuji M., Kenjiro T., Shinsuke T., Takashi K. and Jyunji K.: Quantitative relationship between shape representation quality and calculation accuracy, *Journal of JSCE*, Vol. 70, No. 2, I_519-I_530, 2014.
11) Gregory B. Baecher and John T.: Christian: Reliability and Statistics in Geotechnical Engineering, Wiley, 2005.
12) Cort J. W. and Kenji M.: Advantages of the mean absolute error (MAE) over the root mean square error (RMSE) in assessing average model performance, *Climate Research*. 2005.

(Received May 31, 2024)